Energy Engineering
DOI:10.32604/EE.2020.014016
Article

Analysis of Solar Direct-Driven Organic Rankine Cycle Powered Vapor Compression Cooling System Combined with Electric Motor for Office Building Air-Conditioning

Xiang Xiao[1], Wei Zhao[1], Wei Wang[1], Wei Zhang[1], Xianbiao Bu[2], Lingbao Wang[2,*] and Huashan Li[2]

[1]Electric Power Research Institute of Guangdong Power Grid Co., Ltd., Guangzhou, 510640, China
[2]Guangzhou Institute of Energy Conversion, Chinese Academy of Sciences, Guangzhou, 510640, China
[*]Corresponding Author: Lingbao Wang. Email: wanglb@ms.giec.ac.cn
Received: 28 August 2020; Accepted: 28 September 2020

Abstract: Solar energy powered organic Rankine cycle vapor compression cycle (ORC-VCC) is a good alternative to convert solar heat into a cooling effect. In this study, an ORC-VCC system driven by solar energy combined with electric motor is proposed to ensure smooth operation under the conditions that solar radiation is unstable and discontinuous, and an office building located in Guangzhou, China is selected as a case study. The results show that beam solar radiation and generation temperature have considerable effects on the system performance. There is an optimal generation temperature at which the system achieves optimum performance. Also, as a key indicator, the cooling power per square meter collector should be considered in the hybrid solar cooling system in design process. Compared to the vapor compression cooling system, the hybrid cooling system can save almost 68.23% of electricity consumption.

Keywords: Solar cooling; organic Rankine cycle; vapor compression cycle; hybrid solar cooling system; office building air-conditioning

Nomenclature

A_{col}	collector area, m^2
COP_{VCC}	coefficient of performance for VCC
$COP_{ORC,VCC}$	coefficient of performance for ORC/VCC
G_B	direct radiation intensity, W/m^2
h_1	enthalpy at expander inlet, kJ/kg
h_{2s}	enthalpy at expander outlet based on isentropic process, kJ/kg
h_3	enthalpy at working fluid pump inlet, kJ/kg
h_4	enthalpy at working fluid pump outlet, kJ/kg
h_{4s}	enthalpy at working fluid pump outlet based on isentropic process, kJ/kg
h_5	enthalpy at evaporator outlet, kJ/kg
h_{6s}	enthalpy at compressor outlet based on isentropic process, kJ/kg
h_8	enthalpy at evaporator inlet, kJ/kg
m_{vcc}	mass flow rate for VCC, kg/s

m_{ORC}	mass flow rate for ORC kg/s
P_5	pressure at compressor inlet, kPa
P_6	pressure at compressor outlet, kPa
Q_{gen}	generator heat input, kW
$Q_{em,eva}$	cooling power from electric motor, kW
$Q_{VCC,eva}$	cooling power from solar energy, kW
Q_{eva}	total cooling power from office building, kW
SPC	cooling power per square meter collector, W/m^2
T_{gen}	generation temperature in the generator, °C
T_{con}	condensation temperature, °C
W_{com}	compressor work input from ORC, kW
W_{em}	electric motor work input in ORC/VCC, kW
W_{exp}	expander work output, kW
W_{pp}	working fluid pump power consumption, kW
W_{net}	net work output for ORC, kW
$W_{com,all}$	electric motor work input without solar energy, kW
η_{com}	compressor isentropic efficiency
η_{em}	electric motor efficiency
η_{exp}	expander isentropic efficiency
η_{ORC}	organic Rankine cycle efficiency
η_{pp}	working fluid pump isentropic efficiency
η_{col}	thermal efficiency of solar collector
η_{sys}	overall efficiency of solar cooling system
ΔT	temperature difference of inlet and outlet of collector, °C

1 Introduction

The energy consumption used for air-conditioning has increased drastically in recent years [1]. China has abundant solar energy resources and more than two-thirds of areas receive an annual total solar radiation that exceeds 5.9 GJ/m^2 with sunshine duration more than 2200 h [2]. The utilization of solar energy for cooling is one of the most important measures to reduce fossil fuel consumption [3,4].

Thermally activated cooling technologies have been reported by many researchers [5–11]. Among them, sorption refrigeration cycle and the organic Rankine cycle vapor compression cycle (ORC-VCC) are used to convert solar energy into cooling processes [12–19]. Currently, the use of thermal energy to drive an ORC-VCC system has been reported by several investigators [20–24]. Bu et al. [25] developed an ORC-VCC ice maker driven by solar energy and four working fluids were evaluated to identify the suitable working fluids yielding the highest system efficiency. Salim et al. [26] conducted the multi-objective optimization of an ORC-VCC system driven by the heat source temperatures ranging from 120 to 150°C. Yılmaz [27] investigated the ORC-VCC system for intercity bus air-conditioning using engine exhaust heat with R134a and R245fa as working fluids. Kutlu et al. [28] investigated the heat storage sizing and flow control for a domestic scale solar-powered ORC-VCC system with evacuated flat plate collectors. Moles et al. [29] evaluated the performance of a combined ORC and VCC system activated by low temperature heat sources. Chang et al. [30] proposed a residential combined cooling, heating and power system based on proton exchange membrane fuel cell (PEMFC) and solar energy, consisting of a PEMFC subsystem, an ORC subsystem, domestic hot water subsystem and a VCC subsystem. He et al. [31] analyzed the performance of a desalination system through mechanical vapor compression, coupling with an ORC to drive the steam compressor. What is more, the integrated mechanisms of the coupled desalination system

are demonstrated based on the first and second law of thermodynamics. Li et al. [32] evaluated and analyzed the performance of an ORC-VCC system with the hydrocarbons, including propane, butane, isobutane and propylene, as working fluids. Nasir et al. [33] described the thermal performance of several combinations of working fluids in the ORC-VCC for the domestic air conditioning. Kim et al. [34] carried out a thermodynamic analysis of power/refrigeration cogeneration system activated by low-grade sensible energy. Saleh [35] investigated the thermodynamic performance of an ORC-VCC system from the viewpoint of energy and exergy analysis. Bao et al. [36] compared four different systems using the single-fluid and dual-fluid to evaluate the applicability and six working fluids are analyzed for heat activated cooling systems.

The solar ORC-VCC systems convert solar heat into cooling effect, accomplished by utilizing a Rankine cycle to generate the shaft work to drive a vapor compression cycle. The ORC-VCC provides an alternative to solar cooling besides absorption and adsorption cooling. However, due to the unstable and discontinuous characteristics of solar energy, the back-up source or heat storage equipment are required to ensure smooth operation of solar cooling system, resulting in a high engineering cost. To solve this problem, a hybrid solar energy and electric motor cooling system is proposed in this study. In the hybrid cooling system, solar energy powered ORC and electric motor are operated in parallel, and the problem of unstable and discontinuous energy supply for solar energy can be solved by using electric motor even solar collectors do not work on rainy days. The main aim of this study is to evaluate and analyze the performance of an office building air-conditioning using the ORC-VCC system driven by solar energy combined with electric motor. R245fa is selected as the working fluid and its thermophysical properties are listed in Tab. 1.

Table 1: Thermophysical properties of R245fa

Fluid type	Molecular mass (kg/kmol)	Critical temperature (°C)	Critical pressure (kPa)	Normal boiling point (°C)	Ozone depletion Potential	Global warming Potential
Dry	134.05	154.01	3651.00	15.14	0	950

2 System Description and Thermodynamic Analysis

2.1 System Description

The schematic diagram of the solar ORC-VCC system is presented in Fig. 1. It mainly consists of solar collector (generator), expander, flexible coupling, compressor, frequency conversion motor, condenser 1, throttle valve, evaporator, condenser 2 and working fluid pump.

To yield high system efficiency, the parabolic trough collector is selected to collect solar energy. The R245fa absorbs the solar energy collected by the parabolic trough collector and is vaporized to saturated or superheated vapor in the solar collector. The high pressure vapor drives an expander attached to a vapor compressor. The exhaust working fluid from the expander is condensed into liquid in the condenser 2 by the heat sink. The liquid R245fa is then pumped back to the solar collector. For VCC, the vaporized R245fa from the evaporator flows into compressor and becomes high pressure vapor through compression process. And then the high pressure vapor is cooled down in the condenser 1. Through throttle valve, the liquid R245fa evaporates in the evaporator and generates refrigeration effect. In addition, a frequency conversion motor is used to generate shaft work to drive the compressor. Solar powered ORC and the variable-frequency motor are connected in parallel, and the variable-frequency motor will start when the cooling needs for building cannot be satisfied completely by solar energy.

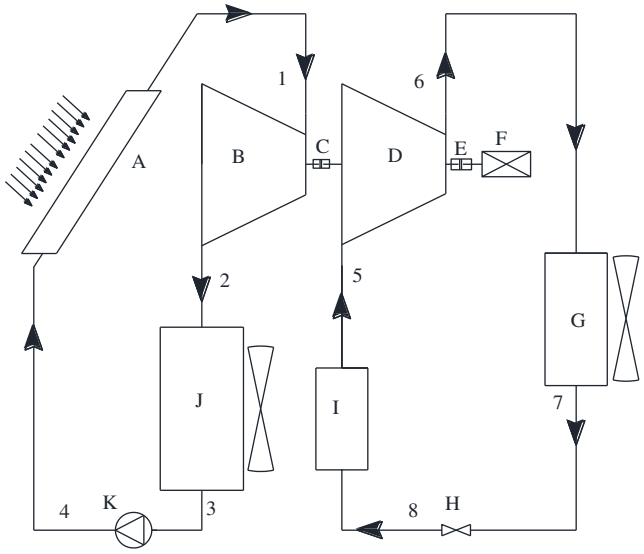

Figure 1: Schematic diagram of hybrid cooling system. A-solar collector (generator), B-expander, C- flexible coupling, D-compressor, E-flexible coupling, F-frequency conversion motor, G-condenser 1, H-throttle valve, I-evaporator, J-condenser 2, K-working fluid pump

2.2 Thermodynamic Analysis

To simplify the mathematical model, some assumptions have been made as follows:

1) Steady-state conditions are considered.
2) Heat and friction losses in the system are neglected.
3) Working fluid leaving the generator, evaporator and condenser is saturated.

Based on these assumptions and referring to the system presented in Fig. 1, the output work of the expander is given by:

$$W_{\text{exp}} = m_{\text{ORC}}(h_1 - h_{2s})\eta_{\text{exp}} \tag{1}$$

where W is output power, kW; m is the mass flow rate, kg/s; h is the specific enthalpy, kJ/kg; η is the isentropic efficiency. The subscripts "exp," "ORC" and "s" denote the expander, ORC subsystem and isentropic process, respectively.

The power consumption of the working fluid pump is expressed by:

$$W_{\text{pp}} = m_{\text{ORC}} \frac{(h_{4s} - h_3)}{\eta_{\text{pp}}} \tag{2}$$

where the subscript "pp" represents working fluid pump.

The useful energy gained from the solar collector, i.e., generator, is calculated from:

$$Q_{\text{gen}} = m_{\text{ORC}}(h_1 - h_4) \tag{3}$$

where Q is the heat transfer rate, kW; the subscript "gen" denotes the generator.

The net power output of the ORC is given by:

$$W_{\text{net}} = W_{\text{exp}} - W_{\text{pp}} \tag{4}$$

where the subscript "net" represents the net power.

The thermal efficiency of the ORC system is defined as follows:

$$\eta_{\text{ORC}} = \frac{W_{\text{net}}}{Q_{\text{gen}}} \tag{5}$$

Note that the shaft of the expander in the ORC and the compressor in the VCR cycle are directly coupled. The output power of the expander is equal to the input power of the compressor, i.e.,

$$W_{\text{com}} = W_{\text{exp}} = m_{\text{VCC}} \frac{(h_{6\text{s}} - h_5)}{\eta_{\text{com}}} \tag{6}$$

where the subscripts "com" and "VCC" represent the compressor and VCC subsystem, respectively.

The cooling power produced from the solar energy is expressed as:

$$Q_{\text{VCC,eva}} = m_{\text{VCC}}(h_5 - h_8) \tag{7}$$

where the subscript "eva" indicates evaporator.

The coefficient of performance of the VCC is given by:

$$\text{COP}_{\text{VCC}} = \frac{Q_{\text{eva}}}{W_{\text{com}}} \tag{8}$$

The coefficient of performance (COP) of the ORC-VCC is given by:

$$\text{COP}_{\text{ORC-VCC}} = \eta_{\text{ORC}}\text{COP}_{\text{VCC}} \tag{9}$$

The thermal efficiency of the solar collector is determined by:

$$\eta_{\text{col}} = 0.762 - 0.2125\left(\frac{\Delta T}{G_{\text{B}}}\right) - 0.001672\left(\frac{\Delta T^2}{G_{\text{B}}}\right) \tag{10}$$

$$\Delta T = T_{\text{col,ave}} - T_{\text{amb}} \tag{11}$$

where G_{b} is beam solar radiation, W; T is temperature, °C. The subscripts "col" and "amb" indicate solar collector and ambient condition, respectively.

The overall thermal efficiency of the ORC-VCC driven by the solar energy is given by:

$$\eta_{\text{sys}} = \eta_{\text{col}}\text{COP}_{\text{ORC-VCC}} \tag{12}$$

When the cooling power produced by the solar driven ORC-VCC cannot meet the cooling load needed, the electric motor will start working for compensation, which is given by:

$$Q_{\text{em,eva}} = Q_{\text{eva}} - Q_{\text{VCC,eva}} \tag{13}$$

where "em" denotes the electric motor.

The electric consumption by the motor is determined by:

$$W_{\text{em}} = \frac{Q_{\text{em,eva}}}{\eta_{\text{em}} \text{COP}_{\text{VCC}}} \tag{14}$$

The cooling power per square meter collector is calculated as follows:

$$\text{SPC} = \frac{Q_{\text{eva}}}{A_{\text{col}}} \tag{15}$$

where A_{col} is solar collector aperture area, m^2.

3 Results and Discussion

The generation temperature (outlet temperature of solar collector) is set at the range of 80–140°C, the condensation temperature is at 40°C, and the evaporation temperature keeps at a constant temperature of 5°C. The isentropic efficiencies for working fluid pump, expander and compressor are 0.90, 0.85 and 0.80, respectively, and the electric motor efficiency is 0.96. The performance of ORC-VCC driven by solar energy is firstly analyzed and evaluated. And then a case study of office building air-conditioning using ORC-VCC driven by solar energy combined with electric motor is conducted.

3.1 Performance of ORC-VCC Driven by Solar Energy

To evaluate the thermodynamic performance of ORC-VCC driven by solar energy, the intensity of beam solar radiation is set at 600 W/m^2.

Fig. 2 shows the variation of solar collector thermal efficiency with the generation temperature. As can be seen, the thermal efficiency of solar collector decreases with generation temperature, which can be well explained by Eqs. (10), (11). Fig. 3 illustrates the change of the ORC thermal efficiency with the generation temperature. It can be found that the ORC thermal efficiency increases firstly and then decreases with generation temperature, indicating that there is a maximum value of the ORC thermal efficiency with different generation temperature, and the maximum value of the ORC thermal efficiency is 14.37% at generation temperature of 130°C. The input heat in the generator is decreased with the rising generation temperature and constant solar radiation intensity; on the other hand, the enthalpy drop across the expander increases with the increasing generation temperature, and thus leading to a decrease of mass flow rate of ORC. The interaction between these effects results in such variation of the ORC thermal efficiency.

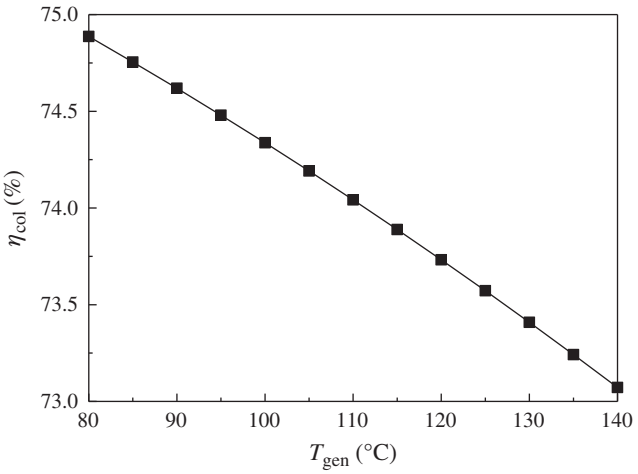

Figure 2: Effect of generation temperature on thermal efficiency of solar collector

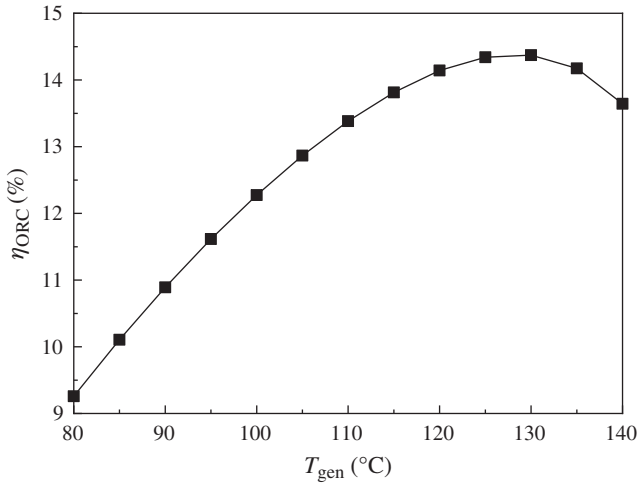

Figure 3: Effect of generation temperature on thermal efficiency of ORC

Fig. 4 exhibits the effect of generation temperature on the COP of the ORC/VCC system. It is well known that the COP for VCC is constant with the fixed condensing temperature and evaporating temperature for VCC. As a consequence, the variation of the COP for ORC-VCC with generation temperature is consistent with the ORC thermal efficiency. The COP of the ORC-VCC obtains the maximum value of 0.73 at the generation temperature of 130°C. As shown in Figs. 5 and 6, although the changing trends of overall efficiency of solar cooling system and cooling power per square meter collector with generation temperature are the same as those of ORC thermal efficiency and the COP for ORC-VCC with generation temperature. The overall thermal efficiency of solar cooling system and cooling power per square meter collector have the maximum value of 53.33% and 319.98 W/m^2, respectively, at the generation temperature of 130°C. This is caused by the comprehensive influence of the solar collector thermal efficiency, ORC thermal efficiency and the COP for ORC-VCC.

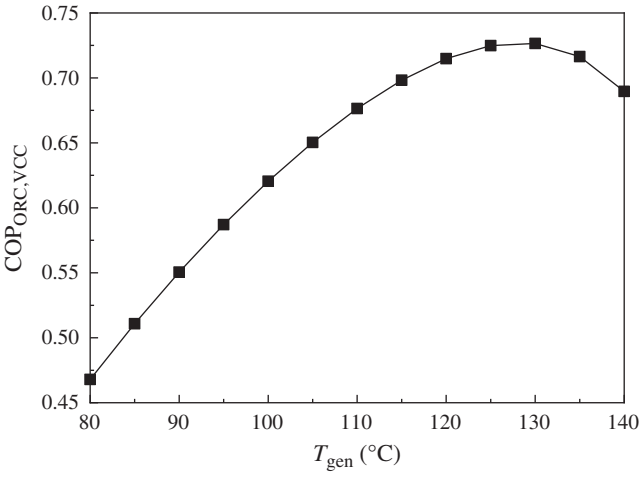

Figure 4: Effect of generation temperature on COP of ORC-VCC

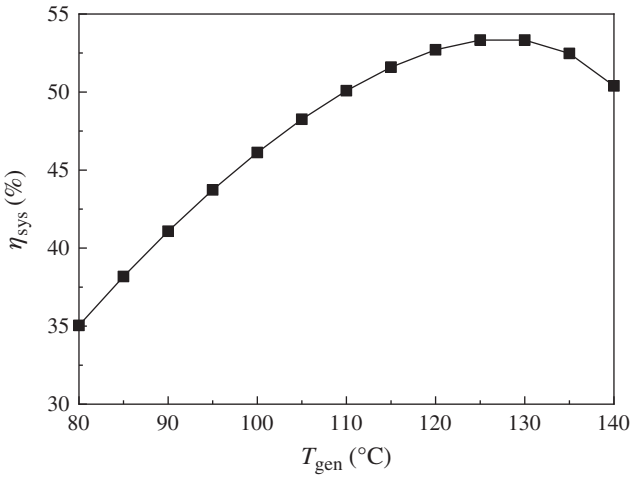

Figure 5: Effect of generation temperature on thermal efficiency of solar powered ORC-VCC

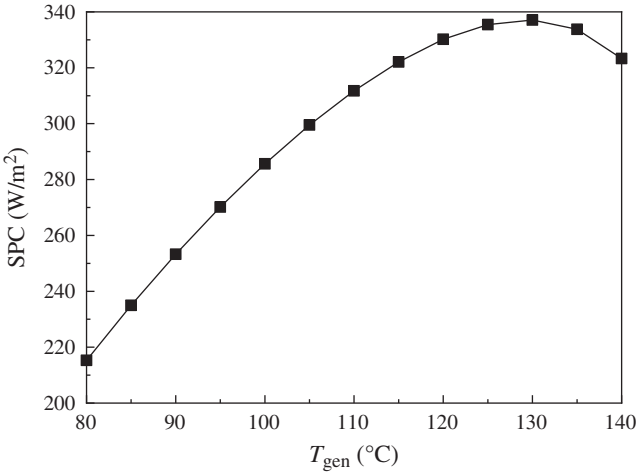

Figure 6: Effect of generation temperature on cooling power per square meter collector

Based on the above result of analysis, it can be concluded that there is the optimal generation temperature, at which the ORC thermal efficiency, COP for ORC/VCC, overall efficiency of solar cooling system and cooling power per square meter collector achieve the maximum values. Therefore, the cooling power per square meter collector should deserve more attention while in the design of the hybrid solar driven cooling system.

3.2 Case Study of Office Building with the Hybrid Solar Cooling System

An office building located in Guangzhou, China is selected as the study subject, and its total construction area is 40000 m^2. The air-conditioning system of office building works from 9:00 to 17:00 every day and its cooling load versus time is depicted in Fig. 7. It shows that the cooling load is low in the morning and lunch break, and it gradually becomes higher in the afternoon. The variations of beam solar radiation and maximum cooling power per square meter collector with time are displayed in Fig. 8. It is obvious that the cooling power per square meter collector depends largely on beam solar radiation intensity, and it is approximately proportional to the solar radiation intensity. With analysis

above, it is concluded that the solar collector with aperture area of 15000 m^2 is required to meet the cooling load of the target building.

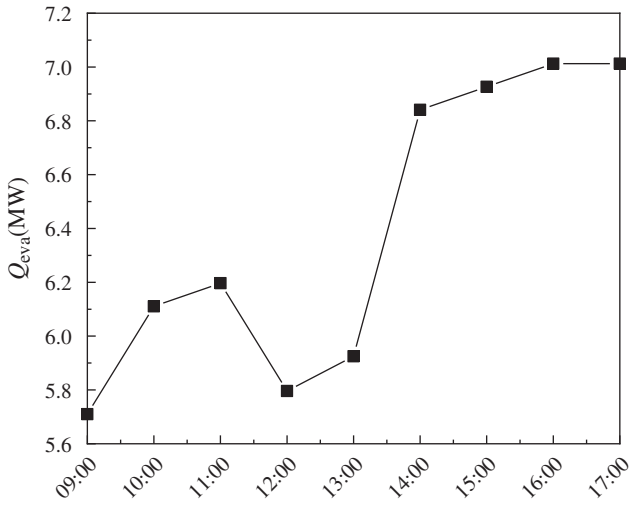

Figure 7: Hourly cooling load of office building

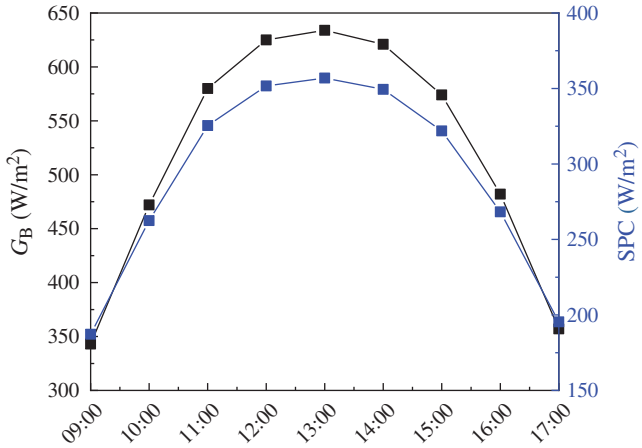

Figure 8: Variation of beam solar radiation and cooling power per square meter collector with time

The variations of $Q_{VCC,eva}$, $Q_{em,eva}$ and Q_{eva} with time are shown in Fig. 9. It can be seen that, the daily average values of $Q_{VCC,eva}$, $Q_{em,eva}$ and Q_{eva} from 9:00 to 17:00 are 4.36 MW, 2.03 MW and 6.39 MW, respectively. That is to say, 68.23% of cooling capacity for the office building is provided by solar energy. Especially at 12:00, solar energy provides 91.01% of the cooling capacity. $Q_{VCC,eva}$ and Q_{eva} have great impacts on $Q_{em,eva}$, and the minimum $Q_{em,eva}$ appears at 12:00 and 13:00, at which $Q_{VCC,eva}$ and G_B have the maximum value, while Q_{eva} has almost the minimum value. The figure also shows that $Q_{em,eva}$ always varies with Q_{eva}, G_B and time. When the cooling capacity provided by solar energy cannot meet the requirement of the whole building cooling load, the electric motor will start to work. Therefore, the programmable logic controller should be installed to adjust $Q_{em,eva}$ according to Q_{eva} and $Q_{VCC,eva}$. By installing the electric motor, the back-up source or heat storage equipment are not required for solar ORC-VCC system, and it can operate stably even solar energy is unstable and discontinuous.

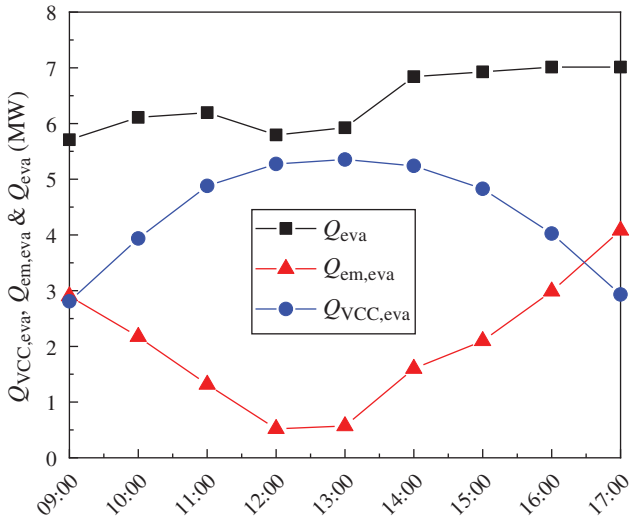

Figure 9: Variation of $Q_{VCC,eva}$, $Q_{em,eva}$ and Q_{eva} with time

The variations of W_{em} and $W_{em,all}$ with time are plotted in Fig. 10, where $W_{em,all}$ indicates the electricity consumption of the compression refrigeration system to meet the cooling load of target building without utilization solar energy. As can be seen from Fig. 10, both W_{em} and $W_{em,all}$ obtain the minimum values at 12:00 and 13:00, which is due to the larger solar radiation intensity as shown in Fig. 8. After 13:00, $W_{em,all}$ increases slowly caused by increased cooling load of office building depicted in Fig. 7. While after 13:00, W_{em} increases significantly owing to the increased cooling load and decreased solar radiation intensity. The daily average values of $W_{tot,em}$ and W_{em} from 9:00 to 17:00 are 1317.33 kW and 417.90 kW respectively, indicating that the electricity consumption saved reaches up to 8094.87 kWh per day.

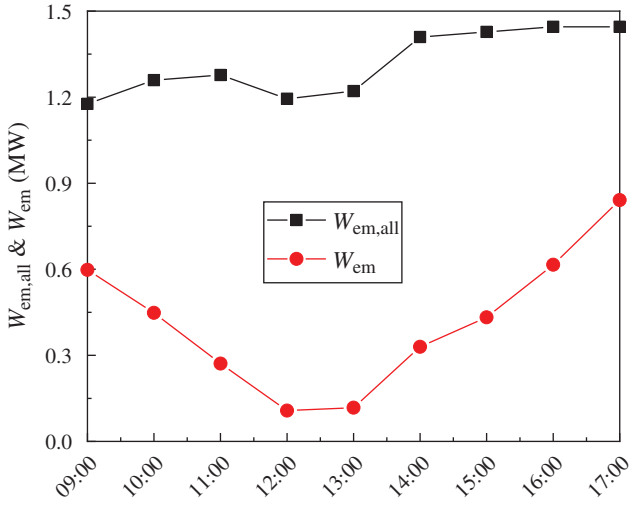

Figure 10: Variation of W_{em} and W_{Tem} with time

4 Conclusions

In this paper, an ORC-VCC system driven by solar energy combined with electric motor is proposed to ensure smooth operation under the conditions that solar radiation is unstable and discontinuous. With an office building located in Guangzhou, China selected as a case study, a thermodynamic model is built to

investigate the thermodynamic performance of the hybrid cooling system. The following conclusions can be drawn:

1. The generation temperature has a considerable influence on the thermodynamic performance of solar ORC-VCC system, which in general increases initially and then decrease with the increased generation temperature. Considering the thermo-economic performance of solar ORC-VCC system, more attention should be paid to cooling power per square meter solar collector.
2. With the addition of electricity motor, the hybrid solar cooling system can operate stably to meet the cooling load for the target building even when solar energy is unstable and discontinuous. The electricity consumption of electric motor is more sensitive to the solar radiation intensity and cooling load. As for the case study, thanks to the solar ORC-VCC system, the electricity consumption saved reaches up to 8094.87 kWh per day.

Moreover, the present paper only focuses on the thermodynamic performance characteristics of solar ORC-VCC under the design conditions. In the future, an off-design analysis should be conducted for reliable and cost-effective operation. Besides, the addition of electricity motor puts forward higher requirements for control strategy research. Also, the power matching and regulation characteristics study should be performed.

Funding Statement: This work was supported by the National Key Research and Development Program of China (No. 2017YFB0903201) and the Science and Technology Project of China Southern Power Grid (No. GDKJXM20172171).

Conflicts of Interest: The authors declare that they have no conflicts of interest to report regarding the present study.

References

1. Martins, M., Mauran, S., Stitou, D., Neveu, P. (2012). A new thermal–hydraulic process for solar cooling. *Energy, 41(1),* 104–112. DOI 10.1016/j.energy.2011.05.030.
2. Li, H. S., Ma, W. B., Lian, Y. Y., Wang, X. L. (2010). Estimating daily global solar radiation by day of year in China. *Applied Energy, 87(10),* 3011–3017. DOI 10.1016/j.apenergy.2010.03.028.
3. Ge, T. S., Wang, R. Z., Xu, Z. Y., Pan, Q. P., Du, S. et al. (2018). Solar heating and cooling: Present and future development. *Renewable Energy, 126,* 1126–1140. DOI 10.1016/j.renene.2017.06.081.
4. Gordon, J. M., Ng, K. C. (2000). High-efficiency solar cooling. *Solar Energy, 68(1),* 23–31. DOI 10.1016/S0038-092X(99)00053-5.
5. Freni, A., Maggio, G., Vasta, S., Santori, G., Polonara, F. et al. (2008). Optimization of a solar-powered adsorptive ice-maker by a mathematical method. *Solar Energy, 82(11),* 965–976. DOI 10.1016/j.solener.2008.05.002.
6. Karamanis, D., Vardoulakis, E. (2012). Application of zeolitic materials prepared from fly ash to water vapor adsorption for solar cooling. *Applied Energy, 97,* 334–339. DOI 10.1016/j.apenergy.2011.12.078.
7. Khattab, N. M. (2004). A novel solar-powered adsorption refrigeration module. *Applied Thermal Engineering, 24 (17–18),* 2747–2760. DOI 10.1016/j.applthermaleng.2004.04.001.
8. Kiplagat, J. K., Wang, R. Z., Oliveira, R. G., Li, T. X. (2010). Lithium chloride—expanded graphite composite sorbent for solar powered ice maker. *Solar Energy, 84(9),* 1587–1594. DOI 10.1016/j.solener.2010.06.014.
9. Laidi, M., Hanini, S. (2013). Optimal solar COP prediction of a solar-assisted adsorption refrigeration system working with activated carbon/methanol as working pairs using direct and inverse artificial neural network. *International Journal of Refrigeration, 36(1),* 247–257. DOI 10.1016/j.ijrefrig.2012.09.016.
10. Leitea, A. P. F., Daguenet, M. (2000). Performance of a new solid adsorption ice maker with solar energy regeneration. *Energy Conversion and Management, 41(15),* 1625–1647. DOI 10.1016/S0196-8904(00)00011-X.

11. Louajari, M., Mimet, A., Ouammi, A. (2011). Study of the effect of finned tube adsorber on the performance of solar driven adsorption cooling machine using activated carbon–ammonia pair. *Applied Energy, 88(3),* 690–698. DOI 10.1016/j.apenergy.2010.08.032.
12. Lu, Z. S., Wang, R. Z., Xia, Z. Z., Lu, X. R., Yang, C. B. et al. (2013). Study of a novel solar adsorption cooling system and a solar absorption cooling system with new CPC collectors. *Renewable Energy, 50,* 299–306. DOI 10.1016/j.renene.2012.07.001.
13. Luo, H. L., Wang, R. Z., Dai, Y. J. (2010). The effects of operation parameter on the performance of a solar-powered adsorption chiller. *Applied Energy, 87(10),* 3018–3022. DOI 10.1016/j.apenergy.2010.03.013.
14. Mateus, T., Oliveira, A. C. (2009). Energy and economic analysis of an integrated solar absorption cooling and heating system in different building types and climates. *Applied Energy, 86(6),* 949–957. DOI 10.1016/j.apenergy.2008.09.005.
15. Rivera, W., Moreno-Quintanar, G., Rivera, C. O., Best, R., Martinez, F. (2011). Evaluation of a solar intermittent refrigeration system for ice production operating with ammonia lithium nitrate. *Solar Energy, 85(1),* 38–45. DOI 10.1016/j.solener.2010.11.007.
16. Patel, B., Desai, N. B., Kachhwaha, S. S. (2017). Thermo-economic analysis of solar-biomass organic Rankine cycle powered cascaded vapor compression-absorption system. *Solar Energy, 157,* 920–933. DOI 10.1016/j.solener.2017.09.020.
17. Vasta, S., Maggio, G., Santori, G., Freni, A., Polonara, F. et al. (2008). An adsorptive solar ice-maker dynamic simulation for north Mediterranean climate. *Energy Conversion and Management, 49(11),* 3025–3035. DOI 10.1016/j.enconman.2008.06.020.
18. Venegas, M., Rodríguez-Hidalgo, M. C., Salgado, R., Lecuona, A. Rodríguez, P. et al. (2011). Experimental diagnosis of the influence of operational variables on the performance of a solar absorption cooling system. *Applied Energy, 88(4),* 1447–1454. DOI 10.1016/j.apenergy.2010.10.011.
19. Wang, L. W., Wang, R. Z., Xia, Z. Z., Wu, J. Y. (2008). Studies on heat pipe type adsorption ice maker for fishing boats. *International Journal of Refrigeration, 31(6),* 989–997. DOI 10.1016/j.ijrefrig.2008.01.002.
20. Aphornratana, S., Sriveerakul, T. (2010). Analysis of a combined Rankine–vapor–compression refrigeration cycle. *Energy Conversion and Management, 51(12),* 2557–2564. DOI 10.1016/j.enconman.2010.04.016.
21. Demierre, J., Henchoz, S., Favrat, D. (2012). Prototype of a thermally driven heat pump based on integrated Organic Rankine Cycles (ORC). *Energy, 41(1),* 10–17. DOI 10.1016/j.energy.2011.08.049.
22. Guo, T., Wang, H. X., Zhang, S. J. (2011). Selection of working fluids for a novel low temperature geothermally-powered ORC based cogeneration system. *Energy Conversion and Management, 52(6),* 2384– 2391. DOI 10.1016/j.enconman.2010.12.038.
23. Stijepovic, M. Z., Linke, P., Papadopoulos, A. I., Grujic, A. S. (2012). On the role of working fluid properties in Organic Rankine Cycle performance. *Applied Thermal Engineering, 36,* 406–413. DOI 10.1016/j.applthermaleng.2011.10.057.
24. Wang, H. L., Peterson, R., Herron, T. (2011). Design study of configurations on system COP for a combined ORC (organic Rankine cycle) and VCC (vapor compression cycle). *Energy, 36(8),* 4809–4820. DOI 10.1016/j.energy.2011.05.015.
25. Bu, X. B., Li, H. S., Wang, L. B. (2013). Performance analysis and working fluids selection of solar powered organic Rankine-vapor compression ice maker. *Solar Energy, 95,* 271–278. DOI 10.1016/j.solener.2013.06.024.
26. Salim, M. S., Kim, M. H. (2019). Multi-objective thermo-economic optimization of a combined organic Rankine cycle and vapour compression refrigeration cycle. *Energy Conversion and Management, 199,* 112054. DOI 10.1016/j.enconman.2019.112054.
27. Yılmaz, A. (2015). Transcritical organic Rankine vapor compression refrigeration system for intercity bus air-conditioning using engine exhaust heat. *Energy, 82,* 1047–1056. DOI 10.1016/j.energy.2015.02.004.
28. Kutlu, C., Erdinc, M. T., Li, J., Wang, Y. B., Su, Y. H. (2019). A study on heat storage sizing and flow control for a domestic scale solar-powered organic Rankine cycle-vapour compression refrigeration system. *Renewable Energy, 143,* 301–312. DOI 10.1016/j.renene.2019.05.017.

29. Moles, F., Navarro-Esbrí, J., Peris, B., Mota-Babiloni, A., Kontomaris, K. (2015). Thermodynamic analysis of a combined organic Rankine cycle and vapor compression cycle system activated with low temperature heat sources using low GWP fluids. *Applied Thermal Engineering, 87,* 444–453. DOI 10.1016/j.applthermaleng.2015.04.083.
30. Chang, H. W., Wan, Z. M., Zheng, Y., Chen, X., Shu, S. M. et al. (2017). Energy analysis of a hybrid PEMFC-solar energy residential micro-CCHP system combined with an organic Rankine cycle and vapor compression cycle. *Energy Conversion and Management, 142,* 374–384. DOI 10.1016/j.enconman.2017.03.057.
31. He, W. F., Ji, C., Han, D., Wu, Y. K., Huang, L. et al. (2017). Performance analysis of the mechanical vapor compression desalination system driven by an organic Rankine cycle. *Energy, 141,* 1177–1186. DOI 10.1016/j.energy.2017.10.014.
32. Li, H. S., Bu, X. B., Wang, L. B., Long, Z., Lian, Y. W. (2013). Hydrocarbon working fluids for a Rankine cycle powered vapor compression refrigeration system using low-grade thermal energy. *Energy and Buildings, 65,* 167–172. DOI 10.1016/j.enbuild.2013.06.012.
33. Nasir, M. T., Kim, K. C. (2016). Working fluids selection and parametric optimization of an Organic Rankine Cycle coupled Vapor Compression Cycle (ORC-VCC) for air-conditioning using low grade heat. *Energy and Buildings, 129,* 378–395. DOI 10.1016/j.enbuild.2016.07.068.
34. Kim, K. H., Perez-Blanco, H. (2015). Performance analysis of a combined organic Rankine cycle and vapor compression cycle for power and refrigeration cogeneration. *Applied Thermal Engineering, 91,* 964–974. DOI 10.1016/j.applthermaleng.2015.04.062.
35. Saleh, B. (2018). Energy and exergy analysis of an integrated organic Rankine cycle-vapor compression refrigeration system. *Applied Thermal Engineering, 141,* 697–710. DOI 10.1016/j.applthermaleng.2018.06.018.
36. Bao, J. J., Zhang, L., Song, C. X., Zhang, N., Zhang, X. P. et al. (2020). Comparative study of combined organic Rankine cycle and vapor compression cycle for refrigeration: Single fluid or dual fluid? *Sustainable Energy Technologies and Assessments, 37,* 100595. DOI 10.1016/j.seta.2019.100595.